Processing and Application of Ceramics 18 [3] (2024) 269–280
https://doi.org/10.2298/PAC2403269Z

The influence of Ti/Ni metallic phase content on the microstructure and environmental interactions of gradient Al_2O_3-based composites

Justyna Zygmuntowicz[1,*], Paulina Piotrkiewicz[1], Marcin Wachowski[2], Radosław Żurowski[3], Anna Więcław-Midor[3], Justyna Tomaszewska-Krygicz[4]

[1]*Warsaw University of Technology, Faculty of Materials Science and Engineering, 141 Woloska St., 02-507 Warsaw, Poland*
[2]*Military University of Technology, Faculty of Mechanical Engineering, gen. S. Kaliskiego 2 St., 00-908 Warsaw, Poland*
[3]*Faculty of Chemistry, Warsaw University of Technology, 3 Noakowskiego St., 00-664 Warsaw, Poland*
[4]*Deloitte Advisory Sp. z o.o., Al. Jana Pawła II 22 St., 00-133 Warsaw, Poland*

Received 16 May 2024; Received in revised form 25 July 2024; Accepted 26 August 2024

Abstract

Al_2O_3/Ti/Ni composites, enhanced with the inclusion of $NiAl_2O_4$ and $TiAl_2O_5$ phases, represent a novel class of advanced materials with multifaceted properties suitable for diverse engineering applications. Centrifugal slip casting method was used for preparation of two series of gradient Al_2O_3/Ti/Ni composite samples with different content of the metallic Ti and Ni phases. Series I containing 0.5 vol.% of Ni and 0.5 vol.% of Ti and Series II containing 2.5 vol.% of Ni and 2.5 vol.% of Ti. Each series contained 55 vol.% of a solid phase. Rheological properties of the suspensions as well as microstructure of the obtained composites were studied, with special attention paid to the analysis of the formed spinel phases. Both series in the green form were characterized by 3-zone structure with different metallic phase content. The widths of individual zones for the Series I and Series II, after sintering at 1450 °C, were 0.53 mm (zone I), 3.26 mm (zone II), 0.8 mm (zone III) and 1.27 mm (zone I), 1.47 mm (zone II), 1.87 mm (zone III), respectively. The results showed that after sintering two spinel phases were formed. The $NiAl_2O_4$ spinel phase consists only of small grains with a size of approximately 1.3–1.8 µm, which form larger clusters with or without a void inside. The $TiAl_2O_5$ phase consists of grains with an average size of 4.3 to 4.5 µm. The Life Cycle Assessment analysis revealed that the values of the global warming potential indicator in phase A1 are 0.16 kg and 0.20 kg equivalent of CO_2 per sintered sample for the Series I and Series II, respectively.

Keywords: *Al_2O_3/Ti/Ni gradient composites, centrifugal slip casting, $NiAl_2O_4$, $TiAl_2O_5$, Life Cycle Assessment*

I. Introduction

In the era of constant search for new materials that meet specific requirements, composites with a ceramic matrix and metallic secondary phase are becoming more and more popular. Compared to single-phase materials, these materials are characterized by low abrasion, high hardness and thermal and chemical resistance while improving resistance to brittle fracture [1,2]. Despite the enormous amount of research work on the formation and characterization of ceramic-metal composites [3,4], they are still the subject of basic research. The reason for this is that many factors can influence the final material. These include, among others, the type and share of the metallic phase, its distribution in the ceramic matrix, as well as its shape and size [5,6]. Thus, many interesting works can be found in the literature on the influence of the particle size on the final product [7,8], the influence of the metallic phase on mechanical properties (i.e. fracture toughness) [9,10] or the influence of metallic additives on the physical and thermal properties of the obtained composites [11,12].

Composites with a ceramic matrix and metallic secondary phase may be characterized by different

*Corresponding author:
e-mail: *Justyna.zygmuntowicz@pw.edu.pl*

microstructures depending on the type and amount of added metal. Nowadays, a lot of attention is paid to functional gradient materials (FGMs). These materials are characterized by a change in the share of the metallic phase in the entire volume of the material [13,14]. This change allows control of the properties of the resulting composite. In particular, it allows the control of the resistance to thermal and mechanical stresses. Moreover, gradient materials are engineered to exhibit tailored variations in composition, microstructure and properties over defined spatial dimensions. Unlike conventional homogeneous materials, FGMs offer unique capabilities to address multifaceted engineering challenges by seamlessly transitioning from one set of properties to another within a single structure. This remarkable attribute has garnered significant attention across diverse scientific and engineering disciplines, ranging from aerospace and automotive industries to biomedical applications. By judiciously tailoring the distribution of constituents, FGMs can achieve enhanced mechanical, thermal, electrical, optical and magnetic properties, surpassing those of conventional homogeneous materials [15–18].

In this work, analysis of the influence of Ti/Ni metallic phase content on the microstructure and environmental interactions of gradient Al_2O_3-based composite was performed. The composites were produced using the centrifugal slip casting (cPC) method, which allows the formation of gradient specimens [10]. Two series of samples were produced, differing in the content of the metallic phase – 1 and 5 vol.%. Each series contained 55 vol.% of the solid phase. Different techniques were used for microstructural characterization of the obtained Al_2O_3/Ti/Ni gradient composites. The work focuses on the detailed analysis of the structure created during the sintering and formation of $NiAl_2O_4$ and $TiAl_2O_5$ spinel phases. Literature data describing this issue indicate a lack of information on a comprehensive description of the morphology of the emerging spinel phase, in particular, the $TiAl_2O_5$ phase. Additional important aspect discussed in this manuscript is the Life Cycle Assessment (LCA) analysis, which allows for the determination of environmental influences accompanying the process of forming Al_2O_3/Ti/Ni composites. Through this manuscript, we aim to stimulate further research and innovation of functional gradient composites with spinel phases, which can contribute to the development of next-generation materials with unprecedented performance and functionality.

To summarize, the results presented in this article are a continuation of the earlier studies on the formation and properties of Al_2O_3/Ti/Ni composites obtained using CSC [10,19]. However, there are differences in several key areas, particularly in terms of the metallic phase content and solid content in the suspension between this article and the previous papers.

II. Experimental

2.1. Sample preparation

Commercially available powders were used: aluminium oxide (TM-DAR from Taimei Chemicals Co., Japan, with an average particle size of 120 ± 30 nm and a density of 3.98 g/cm^3), metallic nickel (Createc, with a density of 8.9 g/cm^3 and an average particle size of <50 μm) and metallic titanium (Alfa Aesar, with a density of 4.5 g/cm^3 and an average particle size of 74 μm). The powder characteristics given above are from safety data sheets obtained from manufacturers.

In this work, two series of gradient samples were prepared, differing in the volume content of the metallic phase (Ti, Ni): Series I containing 0.5 vol.% of Ni and 0.5 vol.% of Ti and Series II containing 2.5 vol.% of Ni and 2.5 vol.% of Ti (the content of the metallic phase was calculated in relation to the total solid phase content). Each of the prepared water-based casting slurries had characterized by 55 vol.% of the solid phase content. The gradient ceramic samples were prepared by using the centrifugal slip casting method, based on the procedure proposed in previous studies and generally accepted in our previous work [10,19,20]. The first stage involved homogenizing the powder mixture in distilled water with deflocculants, using a Retsch ball mill for 30 min at 300 rpm. Deflocculants were chosen based on the literature data [21,22]. Next, the resulting slurry was poured into a gypsum mould, which was then placed inside the centrifuge's metal housing. The mixture was centrifuged at 3000 rpm for 130 min. After demoulding, the sample was dried in a laboratory dryer at 30 °C for 48 h. The final stage was sintering, where the samples were heated at a rate of 2 °C/min to 1450 °C, held for 2 h, and then cooled at 2 °C/min to room temperature. This process was conducted in an HTF 18/04 chamber furnace. The optimized sintering process successfully produced the spinel phase in the Al_2O_3-based composites.

2.2. Characterization

The first stage of the research focused on rheological measurements, carried out using a Kinexus Pro (Malvern Panalytical, Great Britain) rotational rheometer operating in a plate-plate system with a gap height of 0.5 mm at 25 °C. In order to protect the casting masses from drying out at the edges of the measurement geometry, poly(dimethylsiloxane) was spotted on its edges (this substance did not mix with the tested samples). In order to determine the viscosity and flow curves, two-stage measurements of dynamic viscosity and shear stress as a function of shear rate were carried out. In the first stage, measurements were made with an increase in the shear rate from 0.1 to 100 s^{-1}. In the second stage, decreasing shear rate values from 100 to 0.1 s^{-1} were used. The yield stress value of the prepared ceramic slurries was estimated on the basis of data obtained from rotational measurements, during which changes in the

viscosity of the sample were observed with increasing shear stress in the range from 0.1 to 100 Pa.

The manufactured samples (fittings) were subjected to thermogravimetric tests integrated with mass spectrometry in order to characterize the product in its raw state. Raw samples, produced using the centrifugal slip casting method, contain a certain number of organic substances that are released in the form of gases during the sintering process. These gases, when released too rapidly, may cause defects in composites in the form of delaminations or microcracks. Therefore, it is very important to determine the optimal conditions of the sintering process, as well as to investigate the phenomena accompanying the transformations occurring in raw samples when heated to high temperatures, including the sintering temperature. The measurements were carried out using a Netzsch STA 449C thermal analyser integrated with a Netzsch QMS 403C Aeolos mass spectrometer. The mass spectrometer recorded the mass-to-charge ratio (m/z) of ionized molecules in the range of 10–300, as well as their intensity as a function of the increasing temperature during the measurement. The heating rate, final temperature and dwell time at final temperature were 5 °C/min, 1450 °C and 30 min, respectively.

The apparent density, water absorption and open porosity of the composites produced after the sintering process were determined using the hydrostatic method. The linear shrinkage of the samples, which is a manifestation of the sintering process, was calculated as the ratio of the difference in the diameter or length before and after sintering. The volume shrinkage of the produced samples was calculated similarly.

In order to determine the phase composition of the samples in the raw state and after the sintering process, an X-ray diffraction test was performed with Rigaku Mini Flex II diffractometer (Japan). The tests were carried out using CuKα radiation (voltage of 30 kV and intensity of 15 mA) in an angular range of 20°–100°, with a step of $2\theta = 0.05°$ and counting time of 2 s. The PDF+4 2022 pattern database correlated with the Jade 8.5 (Materials Data) program was used to interpret the obtained diffractograms.

Microstructure of the composites was analysed using scanning electron microscope (SEM, JSM-6610) and accelerating voltage of 15 keV. Microscopic observations of the cross-sections of the sintered samples were aimed at determining the distribution of the metallic phase and were made on polished metallographic sections. Before observations, the samples were dusted with a thin layer of carbon. Chemical analysis of microareas was performed using an EDX spectrometer (Oxford X-Max energy-dispersive spectrometer).

Stereological analysis was used to quantitatively and qualitatively describe aluminium oxide particles and the spinel phase in the samples. The analysis was performed using the MicroMeter v.086b computer program [23–25]. The used analysis enabled quantitative description of 3D structures based on a 2D image from SEM micrographs. The analysis was based on binarized images of the microstructure. The equivalent diameter d_2 (the diameter of a circle with the same surface as the surface of the analysed particle or grain was determined), elongation of grains or particles $\alpha = d_{max}/d_2$, convexity of the particles or grains $W = p/p_c$ and curvature of the grain boundary $R = p/(\pi d_2)$ were determined [23–25]. Randomly selected SEM micrographs from areas that had previously been thermally etched were analysed. The composites were thermally etched at 1350 °C for 15 min. Thermal etching of the samples was performed to highlight the boundaries between the grains.

The environmental impacts associated with the formation of ceramic composites with the addition of a metallic phase from the prepared Al_2O_3/Ti/Ni composites were determined using the Life Cycle Assessment (LCA) method, based on the methodology described in the guidelines of the ISO 14044 [26] and EN 15804+A2 [27] standards, in the scope of obtaining and processing raw materials (phase A1) and production of sintered samples (phase A3). The adopted calculation methodology is based on mass allocation. Environmental influences were converted into the declared unit (DU), which in this case is one sintering step with the mass resulting from the recipe. All impacts related to the production of raw materials and additives such as Al_2O_3, Ti, Ni, DAC, CA and deionized water were included in phase A1. The impacts related to the generation and consumption of electricity powering devices used in the sintering process in laboratory conditions were presented in phase A3. Electricity consumption was determined based on operating times and information from manufacturers regarding the maximum power of devices. The energy demand was related to individual stages of the sintering process, based on the entire process and one sintering step (taking into account the size of the furnace chamber, which enables simultaneous sintering of up to 10 samples). The amount of waste from the composite moulding process was estimated at 1.5% of the initial weight loss. Inventory data (LCI) and environmental indicators for LCA calculations were gathered from the Ecoinvent v. 3.10 database (ICPP 2013, Environmental Footprint v. 3.1).

III. Results and discussion

3.1. Rheological properties

Results of rheological properties (Fig. 1) showed quite significant differences in the viscosities of both suspensions. The slurry of Series I (containing 1% of the metallic phase) is characterized by a significantly higher viscosity compared to that of the Series II (containing 5% of the metallic phase) in the entire range of shear rates tested. Moreover, the estimated yield point of the Series I suspension is approximately 19 Pa and is almost 6 times higher compared to the determined yield point of the Series II sample. In one of our previous pub-

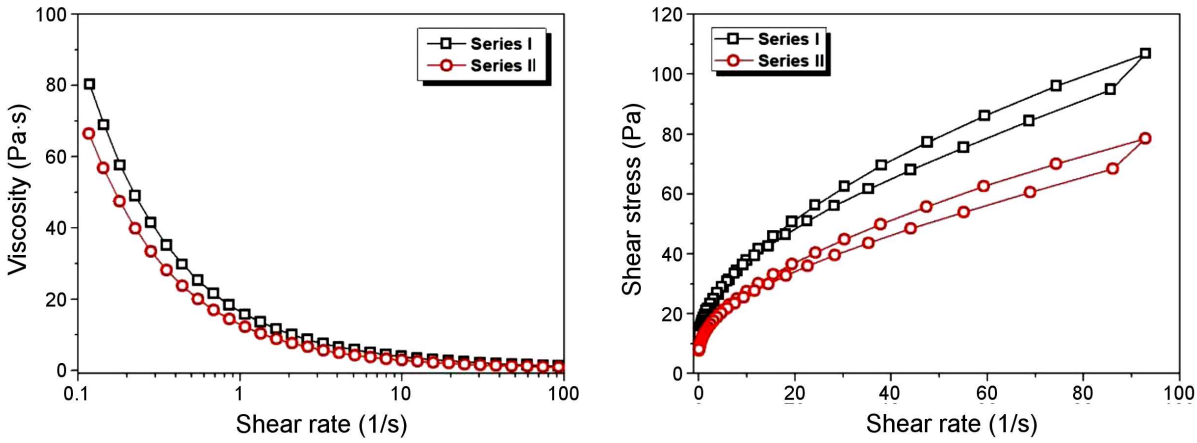

Figure 1. Viscosity curves (a) and flow curves (b) of the prepared ceramic suspensions

lications [10], in which we analysed Al_2O_3/Ti/Ni systems with metallic phase content of 2.5 and 5 vol.%, a higher viscosity was also observed within the sample containing lower content of the metallic phase. It is worth pointing out, however, that the studies mentioned above analysed systems with a much smaller total solid phase (50 vol.%). Hence, the differences were not that clear.

The high solid phase content in the suspensions (55 vol.%) results in relatively high viscosities. Even in the range of high shear rates, the viscosity is approximately 1 Pa·s, which is approximately 5 times higher than in the case of aqueous nano-Al_2O_3/Ti/Ni systems with a solid phase content of 50 vol.% [10,19]. Such high viscosity may significantly limit the process of particle movement during the formation of materials using the CSC method, which consequently could make it difficult to obtain a model gradient structure.

3.2. Thermal analysis

The next stage of the research focused on thermogravimetry analysis. In Fig. 2 DTA/TG curves of thermal degradation of the Al_2O_3/Ti/Ni sample containing 55 vol.% alumina powder and 1 vol.% metallic phase (Ti and Ni) were shown. It indicates that the total mass change was 0.74%. According to the TG curve, it has two main stages (mass losing and mass increasing). The first one begins at ~80 °C and ends at ~480 °C. The mass loss equals 0.56%, ascribed to the dehydration process and the decomposition of the organic phase (citric acid and diammonium citrate). During the second step, in the temperature range of 700–1170 °C, the mass increases (1.30%) which can be ascribed to the creation of oxides and spinel phases ($NiAl_2O_4$ or $TiAl_2O_5$).

The differential thermal analysis (DTA) curve exhibits both endothermic and exothermic peaks. The minimum occurs at 87.8 °C, while the maximum is observed at 814.8 °C. The initial peak can be attributed to the dehydration process. At higher temperatures (above 800 °C), a broad peak emerges. This peak corresponds to mass changes resulting from transformations between the components of the metallic phase and alumina. Mass spectrometry reveals that two main m/z (mass-to-charge ratio) values are 18 and 44. The m/z value 18 corresponds to H_2O molecules (as shown in Fig. 2b). Plotting m/z 18 against temperature reveals a single peak with a maximum of 103.4 °C. Consequently, the primary gaseous product released from the composite sample is water. Additionally, the presence of CO_2 is confirmed by the m/z value 44. Notably, the intensity of the

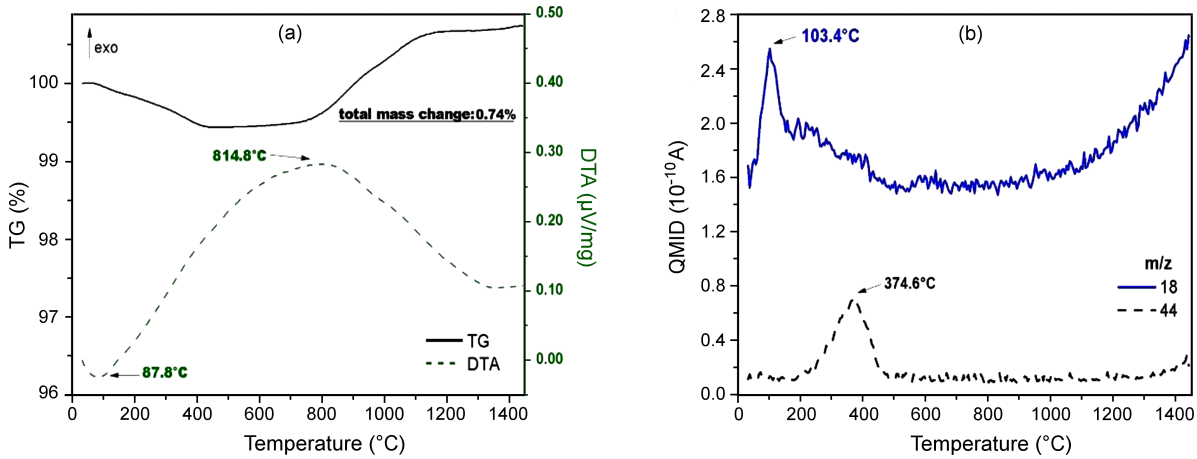

Figure 2. DTA/TG curves (a) and m/z signals (b) of Al_2O_3/Ti/Ni containing 1 vol.% of metallic phase

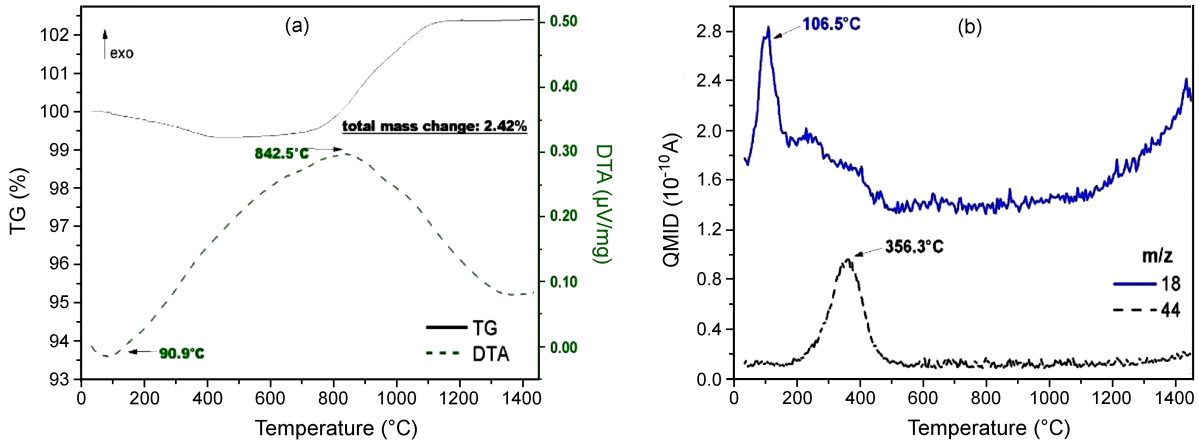

Figure 3. DTA/TG curves (a) and *m/z* signals (b) of Al_2O_3/Ti/Ni containing 5 vol.% of metallic phase

m/*z* 44 signal increases significantly, reaching its peak at 374.6 °C. This phenomenon indicates the decomposition of the organic phase and the oxidation of its products (such as light hydrocarbons) into CO_2.

Thermal degradation (TG and DTA curves) of the sample with 5 vol.% metallic phase (Fig. 3a) indicates that total mass change is 2.42%. On the TG curve, two distinct steps are visible, one with decreasing mass and another with increasing mass (3.09%). Mass loss begins at 90 °C and continues until approximately 500 °C (equivalent to 0.67% mass loss). Interestingly, this behaviour is comparable to the sample containing 1 vol.% of metallic phase. This suggests that both the organic phase decomposition and the dehydration process occur within the same temperature range for both series of samples. However, the mass increasing process (3.09%) starts at ~500 °C and ends at ~1184 °C. The total increase in mass exceeds twice that observed for the sample with 1 vol.% of Ti/Ni.

The endothermic peak on the DTA curve with the minimum at 90.9 °C and the broad, exothermic peak with the maxima at 842.5 °C are visible. The *m*/*z* signal 44 with the maxima at 356.3 °C indicates the decomposition of the organic compound towards CO_2. The highest intensity of *m*/*z* signal 18 is observed at the temperature of 106.5 °C, which can be ascribed to the dehydration process (Fig. 3b). The highest rate of mass change is observed in the temperature range of 90–400 °C. It corresponds to the *m*/*z* 18 and 44 intensity. The last stage of the composite sample degradation is observed in the temperature range 500–1200 °C, where the mass significantly increases, and on the DTA curve, one broad peak is visible. This stage can be ascribed to the creation of oxide spinel phases ($NiAl_2O_4$ or $TiAl_2O_5$).

3.3. Microstructure of Al_2O_3/Ti/Ni composites

The colour change of the heat treated samples is presented in Fig. 4. The sample containing more metallic phase is characterized by more intense grey colour (in the case of the green body) and turquoise colour (in the case of the sintered sample). The composite fittings, produced using the centrifugal slip casting method, are shown in Fig. 5. Macroscopic observations of the raw samples did not reveal any surface defects. After the sintering process, it was found that the sample from Series I was characterized by the lack of delaminations and cracks on the surface. However, in the case of the sample containing 5 vol.% of the metallic phase (Series II), cracks were observed on the surface and inside the pipe. Most likely, the cracks are the result of a large difference in the thermal expansion coefficients of the used components: $\alpha_{Ni} = 13.3 \times 10^{-6}\ °C^{-1}$, $\alpha_{Al_2O_3} = 8 \times 10^{-6}\ °C^{-1}$

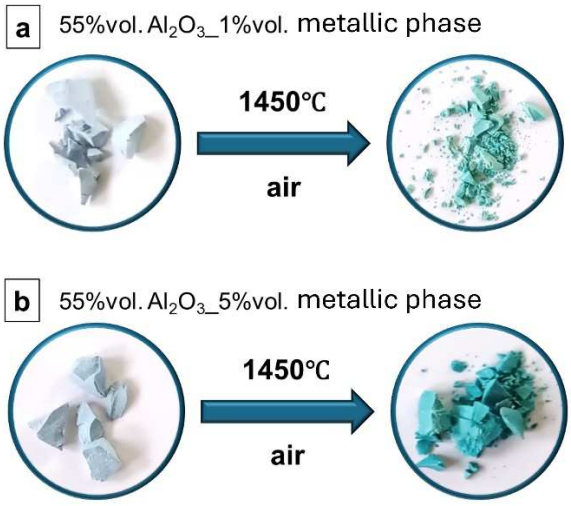

Figure 4. The colour change of heat treated sample

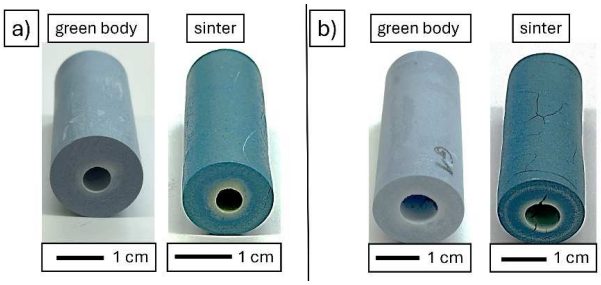

Figure 5. Composite product of the Al_2O_3/Ti/Ni system in the shape of a sleeve, manufactured using the centrifugal slip casting method: a) Series I, b) Series II

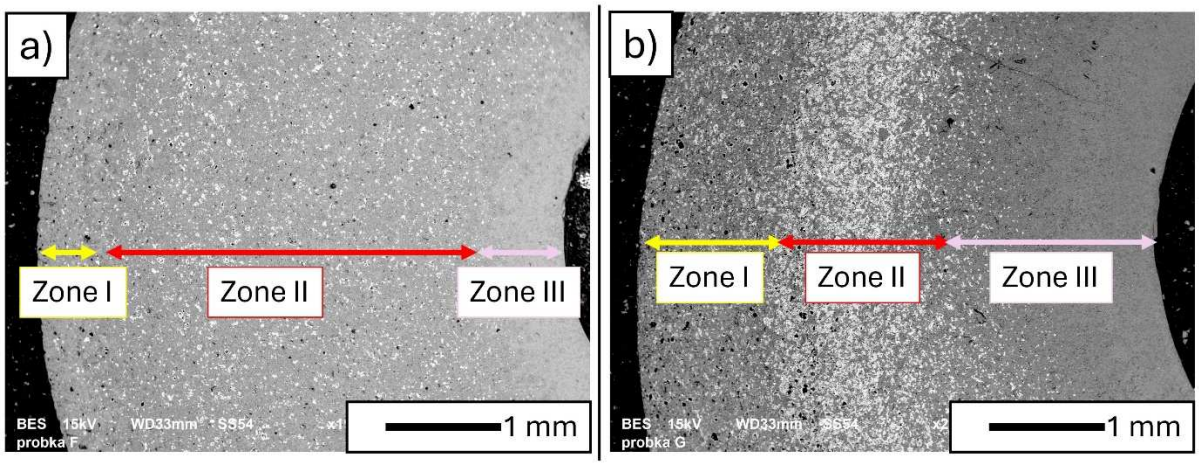

Figure 6. Cross-sections SEM images of sintered Al_2O_3/Ti/Ni fittings: a) Series I and b) Series II

and $\alpha_{NiAl_2O_4} = 8.47\times10^{-6}\,°C^{-1}$ [28–32]. In addition, the sintered samples were turquoise in colour and this may indicate the presence of nickel aluminate in the obtained composites [10,19,33–35]. Thus, since the obtained fittings contain a spinel phase in the form of nickel aluminate, it can be assumed that each mole of Ni reacts in the presence of O_2 with one mole of Al_2O_3, resulting in a significant increase in the volume of the unit cell from $V_{Ni} = 10.93\,Å^3$ to $V_{NiAl_2O_4} = 65.16\,Å^3$ [36].

After the centrifugal casting process of the slurry from Series II higher concentration of the metallic phase was expected in the surface layer. Consequently, this may result in the non-uniformity during the sintering and different material densities in the cross-section. Depending on the content of the metallic phase in individual parts of the sample, the sintering process takes place with different intensities in the surface layer and the sample core, which may result in a state of stress that favours the formation of cracks along the composite core, which was the case for Series II (Fig. 5b).

Based on the results obtained by the hydrostatic method, it was found that the density of composites containing 1 vol.% of the metallic phase (Series I) was 96.05 %TD. However, in the case of composites containing 5 vol.% of the metallic phase (Series II), the density was 92.32 %TD. The lower density of the samples containing more metallic phase (Series II) is most likely the result of the presence of a higher content of the spinel phase after the sintering process.

The volume shrinkages of the samples from Series I and Series II were 28.84 ± 0.03%, and 24.49 ± 1.11%, respectively. However, the linear shrinkage measured in relation to the length of the sample for Series I was 11.32±0.29%, and for Series II was 8.98±0.29%. In the case of linear shrinkage measured relative to the outer diameter of the composite, it was 10.79 ± 0.33% for Series I and 8.95 ± 1.02% for Series II. Based on the obtained results, it was concluded that increased amount of metallic phase resulted in a decrease in the volumetric and linear shrinkages of the fittings. This is most likely due to the fact that the increase in the metallic phase limited the growth of alumina grains during the sintering process. Moreover, the shrinkage values may also be influenced by the content of the spinel phase in the produced samples. It was found that the obtained shrinkage values are slightly lower than those obtained for the composites with a lower solid phase content (50 vol.%) obtained in our previous study [10].

SEM micrographs showing cross-sections of the Al_2O_3/Ti/Ni composites after the sintering (Fig. 6) confirm formation of gradient microstructure in both series. According to our previous publications [10,19,37,38], composites formed using the centrifugal slip casting method were characterized by a conventionally adopted zoned microstructure with 3 distinguished zones. It was observed that, depending on the content of the metallic phase in the composites produced, the width of individual zones varies. The area marked as Zone I is part of the fitting from the outer surface to the area rich in metallic components. Zone I is created when the cast mass was placed in the plaster mould before starting the centrifugal casting process. However, it is advisable to bear in mind the fact that during the process of producing composites using the centrifugal slip casting method, a certain time passes before the cast mass is placed in the plaster mould. This time is necessary to properly perform the process activities, which include pouring and placing the suspension in the plaster mould. It is the use of a plaster mould that allows water to be removed from the cast mass using capillary forces. As a result of using a porous form, the suspension thickens. Consequently, the cast mass used takes the shape of the mould into which it is poured to form a spot in the first stage of the centrifugal slip casting process. Our own research shows that the thickness of this "skin" is proportional to the time it can take to form before the casting process begins [39]. Therefore, free migration of particles during the centrifugal casting of cast masses is no longer possible in the formed "skin". The thickness of the "skin" is an integral element of Zone I. In Zone I, it can be assumed that the solvent moving towards the porous form causes the smallest particles (ceramic)

to move relative to the larger (metallic) particles. This leads to the enrichment of the surface of Zone I with Al_2O_3 particles. Moreover, after starting the centrifugation, the action of centrifugal force intensifies the flow of liquid and thus favours the movement of small-sized particles. This may also be the mechanism of enrichment of Zone I with alumina particles.

The process of thickening the suspension using the centrifugal casting method takes place from the outer surface and goes into the fitting. Therefore, it can be assumed in the model that a certain density front is moving through the sample. It can be assumed that it is represented by the surface of a cylinder, the radius of which decreases during the casting process. Due to the action of centrifugal force, large particles are blocked at the compaction front, which is the beginning of Zone II. In Zone II, metallic particles are predominant. The width of Zone II is influenced by factors such as the mutual speed of movement of individual particles in the mass, depending on their mass and size, as well as the rotational speed of the mould and the speed at which the pour mass is compacted along the radius of the fitting (i.e. the speed of movement of the compaction front) [38,39]. In Zone II, the share of the metallic phase decreases towards the sample axis. Then, Zone III is formed, characterized by a negligible content of the metallic phase.

The obtained micrographs of Al_2O_3/Ti/Ni composites (Fig. 6) prove that with the increase in the content of the metallic phase in the cast mass used to prepare the fittings, the width of individual zones in the produced samples changes, which is consistent with previous work on the formation of samples from the Al_2O_3/Ni system with the CSC method [10,19,38]. It was observed that when a lower content of the metallic phase was used (Series I), the widths of Zone I and Zone III were narrower compared to the zones in the composites produced using a higher content of the metallic phase (Series II) (Fig. 6). However, Zone II in the case of using a lower content of the metallic phase (Series I) was wider in relation to Zone II in composites produced using a higher content of the metallic phase (Series II) (Fig. 6). Observations showed that in the case of composites containing 1 vol.% of the metallic phase (Series I), the interface between the conventionally accepted zones was characterized by a gentle connection. In comparison, in the composites containing a larger amount of the metallic phase (Series II), the interface between the zones was "sharp". The tests showed that in the case of Series I, the width of individual zones was 0.53 mm for Zone I, 3.26 mm for Zone II and 0.86 mm for Zone III. However, in the case of Series II, the widths of individual zones were: Zone I – 1.27 mm, Zone II – 1.47 mm and Zone III – 1.87 mm. Regardless of the content of the metallic phase in the composite, both series of samples were characterized by sample width of 4.6 mm measured from the inner edge of the fitting to its outer edge.

3.4. Phase composition of Al_2O_3/Ti/Ni composites

In order to determine the phase composition before and after the sintering process, XRD analysis was performed. The analysis of the Al_2O_3/Ti/Ni samples with 55 vol.% of the solid phase content in the raw state (Fig. 7), regardless of the metallic phase content, showed the presence of starting components: Al_2O_3 (PDF #04-013-1687), Ti (PDF #01-089-3073) and Ni (PDF #04-016-6268). The analysis of the obtained diffractograms identified five peaks coming from the families of Ti crystallographic planes and four peaks coming from the families of Ni crystallographic planes. In the case of Ti phase, reflections coming from the families of crystallographic planes (100), (002), (101), (103) and (112) were found at the 2θ angle values of: 35.513°, 38.736°, 40.511°, 70.787° and 76.724°, respectively, for the sample from Series I. However, in the case of the sample from Series II, the values of the 2θ angle for the same families of planes were 35.417°, 38.651°, 40.379°, 70.872° and 76.600°, respectively.

The XRD analysis of the phase composition of the samples sintered at 1450 °C (Fig. 8) confirmed the presence of new phases. In both series, the presence of reflections originating from Al_2O_3 (PDF #01-073-5928) and two new phases formed during the sintering process – $NiAl_2O_4$ (PDF #04-008-4744) and $TiAl_2O_5$ (PDF #04-011-9497) were found. The analysis identified six peaks coming from the families of $NiAl_2O_4$ crystallographic planes and four reflections corresponding to the

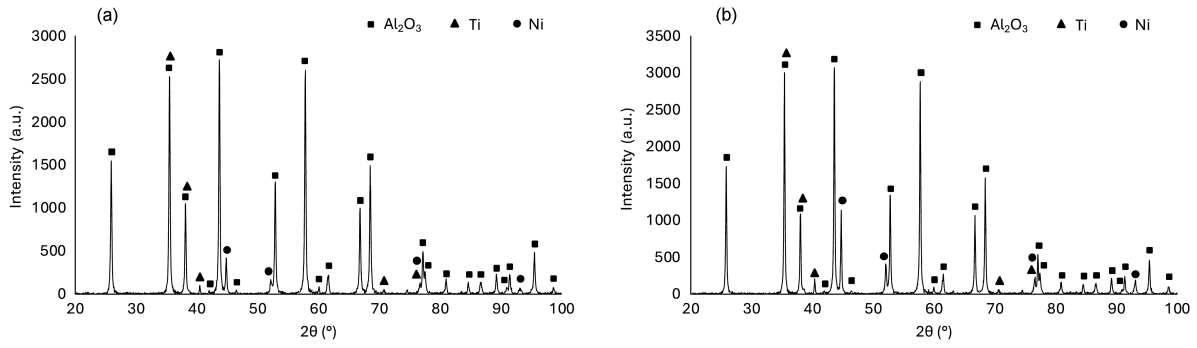

Figure 7. XRD patters of Al_2O_3/Ti/Ni raw mixtures with 55 vol.% of the solid phase content and different metallic phase content: 1 vol.% and b) 5 vol.%

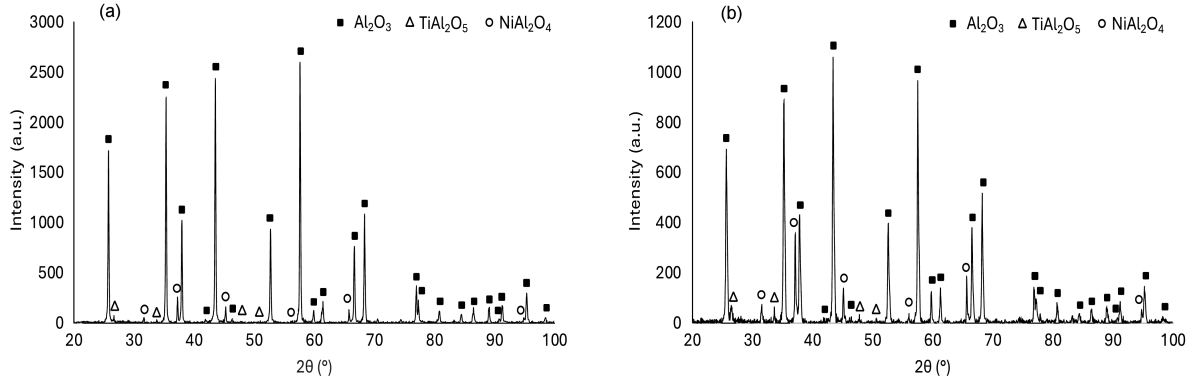

Figure 8. XRD patters of Al_2O_3/Ti/Ni sintered samples with 55 vol.% of the solid phase content and different metallic phase content: 1 vol.% and b) 5 vol.%

families of $TiAl_2O_5$ crystallographic planes. In the case of $NiAl_2O_4$, the identified reflections coming from the families of crystallographic planes (220), (311), (400), (511), (440) and (731) were found at the 2θ angle values of: 31.668°, 37.275°, 45.285°, 59.926°, 65.790° and 94.883° for the samples of Series I and 31.536°, 37.102°, 45.133°, 59.752°, 65.645° and 94.766° for the samples of Series II, respectively. In turn, reflections coming from the families of $TiAl_2O_5$ crystallographic planes (002), (023), (043) and (200) were observed for the 2θ angle values of: 26.686°, 33.878°, 47.937° and 50.695°, respectively, in the case of Series I and 26.453°, 33.621°, 47.902° and 50.607° in the case of Series II, respectively.

The literature data show that the formation of the $NiAl_2O_4$ phase is typically attributed to solid-state reactions between the Al_2O_3 matrix and the Ni during high-temperature processing [40,41]. These reactions involve the diffusion of atoms, phase transformations and chemical reactions, ultimately leading to the formation of the desired $NiAl_2O_4$ phase [42–44]. In the first step, the powders were initially mixed to form homogeneous composite slurries with intimate contact between the Al_2O_3 and Ni phases. In the next stage, the composite mixture was subjected to high-temperature sintering, typically above the melting point of Ni and well within the sintering temperature range of Al_2O_3. During sintering, the powder particles begin to densify and coalesce, promoting atomic diffusion across the Al_2O_3-Ni interface. At elevated temperatures, atomic diffusion occurs within the composite material, allowing Ni atoms to migrate into the Al_2O_3 matrix due to the concentration gradient. As Ni atoms diffuse into the Al_2O_3 matrix, they react with Al atoms to form the $NiAl_2O_4$ spinel phase through a solid-state chemical reaction. This reaction is typically exothermic and proceeds in following way: $2\,Al^{3+} + 4\,NiO \rightarrow NiAl_2O_4 + 3\,Ni^{2+}$; $3\,Ni^{2+} + 4\,Al_2O_3 \rightarrow 3\,NiAl_2O_4 + 2\,Al^{3+}$ [10,19]. The formation of the $NiAl_2O_4$ spinel phase is preferred because of the thermodynamic stability of spinel structure and the affinity of Ni and Al for oxygen. Once initiated, the $NiAl_2O_4$ phase nucleates and grows within the Al_2O_3 matrix, gradually transforming the microstructure of the composite. Crystal growth kinetics, diffusion rates, and local concentration gradients influence the morphology and distribution of the $NiAl_2O_4$ phase within the composite.

In addition to the $NiAl_2O_4$ phase, the $TiAl_2O_5$ phase was also present in the prepared composites. The formation of the $TiAl_2O_5$ phase proceeds in similar way through a combination of solid-state reactions and diffusion processes during the high-temperature processing. Thus, at elevated temperatures, atomic diffusion occurs within the composite material, allowing atoms from different phases to migrate and interact. Titanium atoms diffuse into the Al_2O_3 matrix and nickel phase, while nickel atoms diffuse into the Al_2O_3 and titanium phases. Concentration gradients and thermodynamic forces drive this diffusion process [45,46]. As titanium atoms diffuse into the Al_2O_3 matrix and nickel phase, they can react with Al and Ni atoms to form the $TiAl_2O_5$ phase through solid-state chemical reactions [45,46]. The precise stoichiometry of the reaction may vary, but a representative equation is the following $Al_2O_3 + Ti + Ni + O_2 \rightarrow TiAl_2O_5 + Ni$. The formation of $TiAl_2O_5$ is favoured due to the thermodynamic stability of the compound and the affinity of Ti and Al for oxygen. Once initiated, the $TiAl_2O_5$ phase nucleates and grows within the composite material, gradually transforming the microstructure. Crystal growth kinetics, diffusion rates, and local concentration gradients influence the morphology and distribution of $TiAl_2O_5$ within the composite. Overall, the formation of the $NiAl_2O_4$ and $TiAl_2O_5$ phases in Al_2O_3/Ti/Ni composites involves a complex interplay of diffusion, chemical reactions, and phase transformations influenced by processing parameters such as temperature, time and composition.

In order to confirm the presence of the spinel phases in the prepared composites, a chemical composition analysis (EDX) was performed and the results are presented in Fig. 9. The results obtained showed the presence of four elements: Al, O, Ti, and Ni, thus confirming the presence of $NiAl_2O_4$ and $TiAl_2O_5$ spinel phases, which were shown by the XRD analysis. It may be noted that the compositional analysis with this tech-

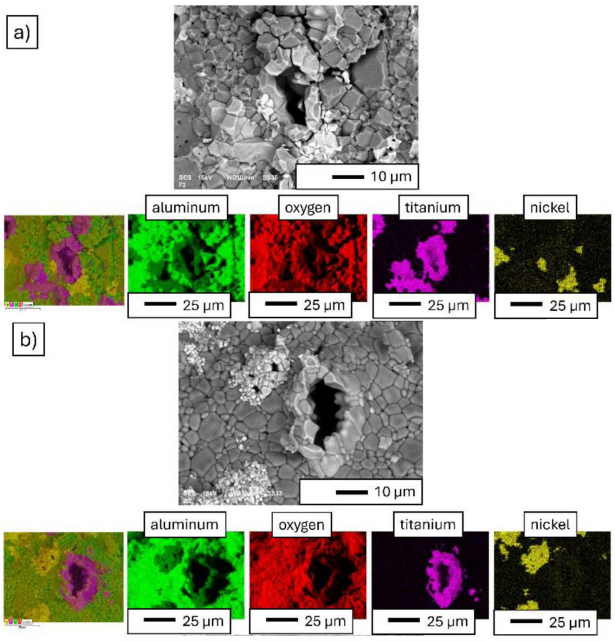

Figure 9. Maps of element distribution in areas containing spinel phases: a) Series I and b) Series II

nique could accurately quantify the Ni, Ti and Al contents within 2–3% error and it is unable to provide an accurate assessment of oxygen content [47]. Based on the previous research [33], it can be concluded that in the case of three-phase Al_2O_3/Ti/Ni composites, the spinel $NiAl_2O_4$ phase has a different morphology than in the case of two-phase Al_2O_3/Ni composites. Thus, in the case of two-phase composites (Al_2O_3/Ni), nickel aluminate is characterized by a two-zone compact microstructure with a void inside. A bimodal distribution characterizes the grains forming the $NiAl_2O_4$ spinel. Large grains are located around the void, and the finer grains forming the $NiAl_2O_4$ spinel are located outside the spinel at the interface with the Al_2O_3 matrix [33]. In the case of Al_2O_3/Ti/Ni composites, it was observed that the $NiAl_2O_4$ spinel phase consists only of tiny grains that are connected into larger clusters with or without a void inside.

Thus, it can be seen that in the case of Series I (1 vol.% of the metallic phase), the $NiAl_2O_4$ grains have size ranging from 0.20 to 8.2 µm, and for the Series II (5 vol.% of the metallic phase) the sizes are in the range from 0.20 to 5.2 µm. It is worth noting that the largest number of $NiAl_2O_4$ grains is in the range from 1.0 µm to 1.2 µm and from 1.0 µm to 1.6 µm in the case of the samples from Series I and Series II, respectively.

The average size of $NiAl_2O_4$ grains was determined by stereological analysis (Fig. 10). Based on the results obtained, it was found that in the case of Series I, the average size of the grains forming the $NiAl_2O_4$ phase was 1.81 ± 1.12 µm, and in the case of Series II, the average size of the grains forming the $NiAl_2O_4$ phase was 1.29 ± 0.71 µm. The obtained histograms have an unimodal distribution regardless of the Series examined (Fig. 10). The analysis showed that an increase in the

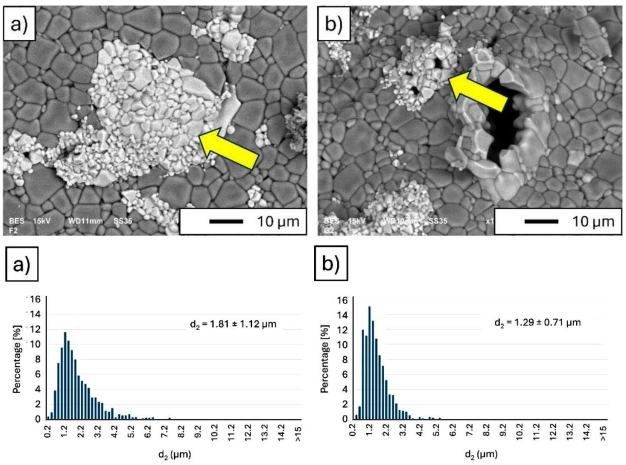

Figure 10. Example of microstructure and histograms showing the distribution of $NiAl_2O_4$ in Al_2O_3/Ti/Ni composites produced by the CSC method: a) Series I – 1 vol.% of the metallic phase, b) Series II – 5 vol.% of the metallic phase

content of the metallic phase in the cast mass results in a small decrease in the average size of $NiAl_2O_4$ grains formed. The shape parameters of the formed $NiAl_2O_4$ grains were also determined and are in the range from 1.07 to 1.31. This proves that the $NiAl_2O_4$ grains have shape close to spherical, which is similar to our previous results [10,19].

Stereological analysis was also utilized to ascertain the mean grain size of the spinel $TiAl_2O_5$ phase (Fig. 11). The findings indicate that for the Series I, the average grain size of the spinel phase is 4.53 ± 3.01 µm, while for the Series II it is 4.23 ± 2.82 µm. The shape parameters of the $TiAl_2O_5$ grains range from 1.09 to 1.45, indicating a near-spherical shape of the spinel $TiAl_2O_5$ grains. Thus, it can be concluded that the metallic phase content does not have significant influence on the size and shape of the formed $TiAl_2O_5$ phase in the composites.

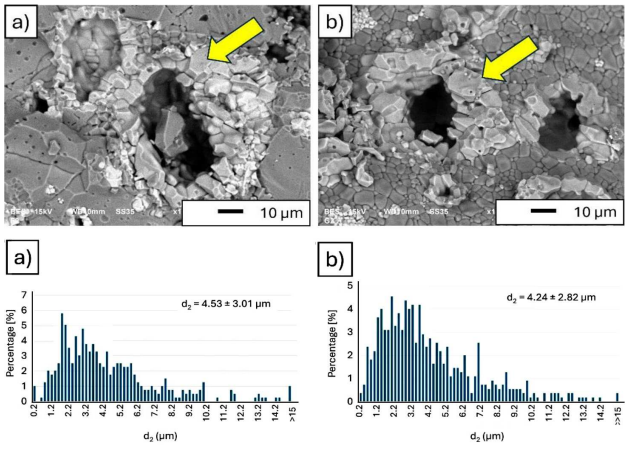

Figure 11. Example of microstructure and histograms showing the distribution of $TiAl_2O_5$ in Al_2O_3/Ti/Ni composites produced by the CSC method: a) Series I – 1 vol.% of the metallic phase, b) Series II – 5 vol.% of the metallic phase

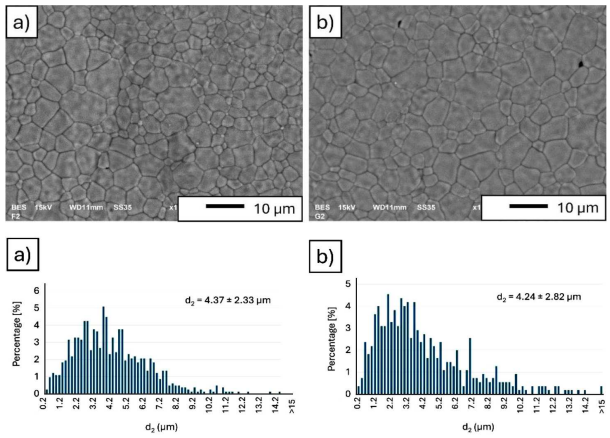

Figure 12. Example of microstructure and histograms showing the distribution of Al_2O_3 in Al_2O_3/Ti/Ni composites produced by the CSC method: a) Series I – 1 vol.% of the metallic phase, b) Series II – 5 vol.% of the metallic phase

The influence of the metallic phase content on the growth of Al_2O_3 grains in the Al_2O_3/Ti/Ni composites was also determined. Figure 12 presents selected micrographs showing Al_2O_3 grains after the thermal etching process, along with histograms showing the size distribution of Al_2O_3 grains (their equivalent diameter, i.e. the diameter of a circle with the same area as the surface of the analysed grain). Based on the analysis, it was found that in the case of Series I (1 vol.% of the metallic phase) and Series II (5 vol.% of the metallic phase) the average size of Al_2O_3 grains were 4.37 ± 2.33 µm and 4.24 ± 2.82 µm, respectively. Interestingly, these values are much higher than the values obtained in our earlier work, where the average Al_2O_3 grain sizes were 3.95 and 2.78 µm for the sample with 2.5% and 5% metallic phase, respectively, but smaller content of the solid phase (50%) [10,19]. Therefore, based on the results obtained, it can be assumed that both the content of the metallic phase and the content of the solid phase in the suspension influence the growth of Al_2O_3 during sintering. The analysis also showed that the content of the metallic phase in the composite does not have influence on the shape of Al_2O_3 grains, which are mostly equiaxial. Analogous conclusions were obtained in our previously published work related to the Al_2O_3/Ti/Ni system containing 50% of the solid phase [10].

3.5. Life Cycle Assessment

Life Cycle Assessment (LCA) of the Al_2O_3/Ti/Ni composites containing 1 vol.% (Series I) and 5 vol.% of the metallic phase (Series II) was performed: i) in the part of obtaining and processing raw materials (phase A1) and ii) the production of sintered materials in a process carried out on a laboratory scale (phase A3). The obtained results indicate that as the content of the metallic phase increases the environmental footprint of the sintered samples in the phase A1 increases, which is a direct consequence of the increased use of raw materials. In the case of the sintered samples from Series I, the value of the global warming potential index is 0.16 kg equivalent of CO_2 per one sintering batch, and for Series II it is 0.20 kg equivalent of CO_2. This is due to the much higher environmental impact of Ti and Ni powders compared to Al_2O_3, which is related to the greater resource and energy consumption of their acquisition and processing methods [48,49]. The implementation of all operations required to produce sintered samples meaning that the duration of the full process is slightly over 21 h. By analysing the energy consumption of the process, it can be seen that the sintering stage is responsible for almost 99% of the energy demand of the process, while the deaeration and centrifugal casting processes are responsible for less than 1.15%. Taking into account the size of the furnace chamber, and therefore the maximum number of samples that could potentially be sintered at the same time, and converting the total energy demand of the process into one sintering batch, it can be seen that the centrifugal casting and sintering processes would be responsible for approximately 8.7% and 89.6% of the energy demand of the process, respectively, and homogenization accounts for the remaining less than 1.6%. In connection with the above, it can be noted that the choice of infrastructure is a key factor determining energy consumption in this laboratory-scale process. Relatively high energy demand per unit of product is typical for processes carried out in non-optimized laboratory conditions. The obtained results clearly indicate the need to perform qualitative and quantitative optimization in terms of the energy demand of the process in the case of composite production on an industrial scale. The conclusions drawn in the authors' previous research [10,19,20] prove that a conscious choice of infrastructure can significantly reduce the impact on the environment generated at the stage of laboratory work, thus leading to a reduction in the environmental footprint of the academic environment and, in the future, of the sector in which the process solution will be implemented. LCA can be considered an effective and low-cost tool enabling the selection of optimal process parameters and supporting the selection of energy-saving and low-emission research infrastructure, supporting the transformation of scientific institutions and R&D activities towards low-emission and in line with the Circular Economy assumptions.

IV. Conclusions

The centrifugal slip casting (CSC) method was used to produce two series of Al_2O_3/Ti/Ni gradient composites containing different Ti/Ni content (Series I with 1 vol.% and Series II with 5 vol.%). Both series were characterized by 3-zone structure with different metallic phase content. The sintered sample with lower Ti/Ni content (1 vol.%) was characterized by the lack of delaminations and cracks on the surface, making CSC a viable alternative for creating gradient composites.

The composites with 1% metallic phase (Series I) achieved a density of 96.05 %TD, whereas those with 5 vol.% of Ti/Ni (Series II) had a density of

92.32 %TD. XRD and EDX analyses confirmed the presence of $NiAl_2O_4$ and $TiAl_2O_5$ phases in both series. The higher metallic content led to the increased spinel phase content after sintering. The metallic phase content influenced the zone widths within the composites. Widths of the Zone I, Zone II and Zone III were 0.53 mm, 3.26 mm 0.8 mm for the Series I, and 1.27 mm, 1.47 mm, 1.87 mm for the Series II. Stereological analysis indicated that higher metallic phase content reduced the average grain size of the $NiAl_2O_4$ and $TiAl_2O_5$ spinel phases and influenced the growth of Al_2O_3 grains post-sintering.

The environmental footprint increased with higher metallic content due to the greater raw material usage. The Series I and Series II had a global warming potential of 0.16 kg and 0.20 kg CO_2 per one sintering batch, respectively. The sintering stage accounted for almost 99% of the total energy demand, highlighting the need for optimization in industrial-scale production, particularly in the sintering process.

Acknowledgements: Studies were funded by the Faculty of Material Science and Engineering, Warsaw University of Technology, within the framework of the research subvention work no. 504/04856/1090/43.082312 - Project Manager: Ph.D. Eng. Justyna Zygmuntowicz.

References

1. T. Rodriguez-Suarez, J.F. Bartolomé, J.S. Moya, "Mechanical and tribological properties of ceramic/metal composites: A review of phenomena spanning from the nanometer to the micrometer length scale", *J. Eur. Ceram. Soc*., **32** (2012) 3887–3898.
2. T. Zhu, Z. Wang, "Research and application prospect of short carbon fiber reinforced ceramic composites", *J. Eur. Ceram. Soc.*, **43** (2023) 6699–6717.
3. J. Xia, T. Ding, W. Ren, X. Zhao, K. Ren, Y. Wang, "Ceramics/metals joining under the influence of electric field: A review", *J. Eur. Ceram. Soc.*, **43** (2023) 5061–5077.
4. Q. Diao, H. Zou, X. Ren, C. Wang, Y. Wang, H. Li, T. Sui, B. Lin, S. Yan, "A focused review on the tribological behavior of C/SiC composites: Present status and future prospects", *J. Eur. Ceram. Soc.*, **43** (2023) 3875–3904.
5. Y. Yu, X. Wang, Y. Wu, M. Ma, G. Gao, "The impact of backplate support conditions on ceramic fracture and energy absorption in the penetration resistance process of ceramic/metal composite armor", *Ceram. Int.*, **50** (2024) 10325–10339.
6. J. Schukraft, D. Horny, F. Siegmund, K. Schulz, K.A. Weidenmann, "Experimental and numerical investigation of the thermal properties and related microstructural influences of an interpenetrating metal ceramic composite at elevated temperatures", *Thermochim. Acta*, **726** (2023) 179557.
7. G. Mathew, V.K.N. Kottur, "Effect of ceramic reinforcements on the mechanical and tribological properties of aluminium metal matrix composites – A review", *Mater. Today Proc.*, in press, 2023.
8. C.R. Mahesha, N. Nithyanandan, K.V. Pradeep Kumar, P. Mishra, S. Singh, H.M. Salman, V. Mohanavel, "Influence of the addition of ZrO_2 powder reinforced with aluminate platelets on the mechanical properties of the ceramic composite", *Mater. Today Proc.*, in press, 2023.
9. J. Tanska, P. Wiecinski, M. Kukielski, J. Zygmuntowicz, P. Wiecinska, "Coordination complexes as substitutes for metallic powders in ceramic-matrix-composites manufactured by aqueous colloidal processing: Enhanced fracture toughness and quantitative microstructure analysis", *J. Eur. Ceram. Soc.*, **44** (2024) 341–352.
10. J. Zygmuntowicz, P. Piotrkiewicz, R. Żurowski, A. Więcław-Midor, P. Falkowski, M. Wachowski, J. Tomaszewska, "The influence of the metallic phase on the microstructure and properties of Al_2O_3/Ti/Ni composites, taking into account environmental influences related to their production", *Ceram. Int.*, **49** (2023) 39147–39162.
11. Q. Chen, M. Yu, K. Cao, H. Chen, "Thermal conductivity and wear resistance of cold sprayed Cu-ceramic phase composite coating", *Surf. Coat. Tech.*, **434** (2022) 128135.
12. M.R. Akbarpour, F. Gazani, H. Mousa Mirabad, I. Khezri, A. Moeini, N. Sohrabi, H.S. Kim, "Recent advances in processing, and mechanical, thermal and electrical properties of Cu-SiC metal matrix composites prepared by powder metallurgy", *Prog. Mater. Sci.*, **140** (2023) 101191.
13. Y. Watanabe, N. Yamanaka, Y. Fukui, "Control of composition gradient in a metal-ceramic functionally graded material manufactured by the centrifugal method", *Compos. A App. Sci. Manuf.*, **29** (1998) 595–601.
14. O. Gillia, B. Caillens, "Fabrication of a material with composition gradient for metal/ceramic assembly", *Powder Technol.*, **208** (2011) 355–366.
15. A.J. Ruys, B.A. Sutton, "9 - Metal-ceramic functionally graded materials (FGMs), Advanced Ceramic Materials", pp. 327–359 in *Metal-Reinforced Ceramics*, Woodhead Publishing, 2021.
16. J. Chang, X. Peng, J. Li, T. Ellis, "Design and fabrication of Ni/ZrO_2 metal-ceramic functionally graded materials by a moving-magnetic-field-driving method", *J. Mater. Res. Technol.*, **13** (2021) 1000–1011.
17. M. Hamamcı, F. Nair, A.A. Cerit, "Microstructural and mechanical characterization of functionally graded Fe/Fe_2B (Fe/B_4C) materials fabricated by in-situ powder metallurgy method", *Ceram. Int.*, **49** (2023) 18786–18799.
18. J. Zang, R. Xiao, Y. Zhang, L. Chen, "A novel way for vibration control of FGM fluid-conveying pipes via NiTiNOL-steel wire rope", *Appl. Math. Mech.-Engl. Ed.*, **44** (2024) 877–896.
19. J. Zygmuntowicz, J. Tomaszewska, M. Wieczorek, R. Żurowski, P. Piotrkiewicz, M. Wachowski, P. Wieciński, "Properties of Al_2O_3/Ti/Ni composites fabricated via centrifugal slip casting under environmentally assessed conditions as a step toward climate-neutral society", *Ceram. Int.*, **48** (2022) 21879–21892.
20. J. Zygmuntowicz, J. Tomaszewska, J. Jeleń, P. Piotrkiewicz, M. Wachowski, J. Torzewski, R. Żurowski, "Comprehensive analysis of the microstructure, properties and environmental performance of Al_2O_3-ZrO_2 composites obtained via centrifugal slip casting", *Chem. Eng. Sci.*, **263** (2022) 118086.
21. M. Gizowska, K. Konopka, M. Szafran, "Properties of water-based slurries for fabrication of ceramic-metal composites by slip casting method", *Arch. Metall. Mater.*, **56** (2011) 1105–1110.
22. P.C. Hidber, T. J. Graule, L. J. Gauckler, "Citric acid - a

dispersant for aqueous alumina suspensions", *J. Am. Ceram. Soc.*, **79** (1996) 1857–1867.
23. J. Michalski, T. Wejrzanowski, R. Pielaszek, K. Konopka, W. Łojkowski, K.J. Kurzydłowski, "Application of image analysis for characterization of powders", *Mater. Sci. Pol.*, (2005) 79–86.
24. T. Wejrzanowski, K.J. Kurzydlowski, "Stereology of grains in nano-crystals", *Solid State Phenom.*, **94** (2003) 221–228.
25. T. Wejrzanowski, W. Spychalski, K. Różniatowski, K. Kurzydłowski, "Image based analysis of complex microstructures of engineering materials", *Int. J. Appl. Mathe. Comp. Sci.*, **18** (2008) 33–39.
26. ISO 14044:2006 Environmental management Life cycle assessment Requirements and guidelines
27. EN 15804:2012+A2:2019 Sustainability of construction works - Environmental product declarations - Core rules for the product category of construction products
28. W.D. Callister, *Materials Science and Engineering*, John Wiley & Sons, USA, 2007.
29. C. Alcázar, R. Moreno, "Manufacture of titania foams by replica method and infiltration with anatase nanoparticles", *Eur. J. Mater.*, **3** (2023) 2225542.
30. P. Falkowski, R. Żurowski, "Shaping of alumina microbeads by drop-casting of the photopolymerizable suspension into silicone oil and UV curing", *J. Eur. Ceram. Soc.*, **42** (2022) 3957–3967.
31. S.S. Hossain, B. Gao, S. Park, C.-J. Bae, "Incorporating nanoparticles in alumina ink for improved solid-loading and sinterability of extrusion-based 3D printing", *ACS Appl. Nano Mater.*, **5** (2022) 17828–17838.
32. B. Inserra, B. Coppola, L. Montanaro, J.-M. Tulliani, P. Palmero, "Preparation and characterization of Ce-ZrO_2/Al_2O_3 composites by DLP-based stereolithography", *J. Eur. Ceram. Soc.*, **43** (2023) 2907–2916.
33. J. Zygmuntowicz, A. Miazga, K. Konopka, "Morphology of nickel aluminate spinel ($NiAl_2O_4$) formed in the Al_2O_3–Ni composite system sintered in air", *Compos. Theory Pract.*, **14** (2014) 106–110.
34. K. Konopka, L. Lityńska-Dobrzyńska, J. Dutkiewicz, "SEM and TEM studies of $NiAl_2O_4$ spinel phase distribution in alumina matrix", *Arch. Metall. Mater.*, **58** (2013) 501–504.
35. J. Zygmuntowicz, P. Wiecińska, A. Miazga, K. Konopka, "Characterization of composites containing $NiAl_2O_4$ spinel phase from Al_2O_3/NiO and Al_2O_3/Ni systems", *J. Therm. Anal. Calorim.*, **125** (2016) 1079–1086.
36. M. Lieberthal, W.D. Kaplan, "Processing and properties of Al_2O_3 nanocomposites reinforced with sub-micron Ni and $NiAl_2O_4$", *Mater. Sci. Eng. A*, **302** (2001) 83–91.
37. J. Zygmuntowicz, A. Miazga, P. Wiecinska, W. Kaszuwara, K. Konopka, M. Szafran, "Combined centrifugal-slip casting method used for preparation the Al_2O_3-Ni functionally graded composites", *Compos. B Eng.*, **141** (2018) 158–163.
38. J. Zygmuntowicz, A. Miazga, K. Konopka, W. Kaszuwara, "Structural and mechanical properties of graded composite Al_2O_3/Ni obtained from slurry of different solid content", *Procedia Struct. Integr.*, **1** (2016) 305–312.
39. R. Żurowski, J. Zygmuntowicz, P. Piotrkiewicz, M. Wachowski, M.M. Szczypiński, "ZTA Pipes with a gradient structure-effect of the rheological the behavior of ceramic suspensions on the gradient structure and characterized of the obtained products", *Materials*, **14** (2021) 7348.
40. N.M. Deraz, "Synthesis and characterization of nano-sized nickel aluminate spinel crystals", *Int. J. Electrochem. Sci.*, **8** (2013) 5203–5212.
41. N. Sahli, C. Petit, A.C. Roger, A. Kiennemann, S. Libs, M.M. Bettahar, "Ni catalysts from $NiAl_2O_4$ spinel for CO_2 reforming of methane", *Catal. Today*, **113** (2006) 187–193.
42. W. Zhang, J.R. Smith, A.G. Evans, "The connection between *ab initio* calculations and interface adhesion measurements on metal/oxide systems: Ni/Al_2O_3 and Cu/Al_2O_3", *Acta Mater.*, **50** (2002) 3803–3816.
43. H. Meltzman, D. Mordehai, W.D. Kaplan, "Solid-solid interface reconstruction at equilibrated Ni-Al_2O_3 interfaces", *Acta Mater.*, **60** (2012) 4359–4369.
44. F.S. Pettit, E.H. Randklev, E.J. Felten, "Formation of $NiAl_2O_4$ by solid state reaction", *J. Am. Ceram. Soc.*, **49** (1966) 199–203.
45. H.J. Seifert, A. Kussmaul, F. Aldinger, "Phase equilibria and diffusion paths in the Ti-Al-O-N system", *J. Alloy. Compd.,* **317-318** (2001) 19–25.
46. C.C. Chen, "Phase equilibria at Ti–Al interface under low oxygen pressure", *Atlas J. Mater. Sci.,* **1** (2014) 1–11.
47. K. Tahmasebi, M.H. Paydar, "Microwave assisted solution combustion synthesis of alumina-zirconia, ZTA, nanocomposite powder", *J. Alloy. Compd.*, **509** (2011) 1192–1196.
48. D. Landi, C. Spreafico, D. Russo, "LCA of titanium powder: empirical evidence vs data from patents, possible future applications", *Procedia CIRP*, **116** (2023) 318–323.
49. L.V.M. Antony, R.G. Reddy, "Processes for production of high-purity metal powders", *JOM*, **55** (2003) 14–18.